ELSEVIER

Cognitive Brain Research 13 (2002) 293–304

COGNITIVE BRAIN RESEARCH

www.elsevier.com/locate/bres

Research report

Collective bursting in layer IV Synchronization by small thalamic inputs and recurrent connections

Ruedi Stoop[a,*], Daniel Blank[a], Albert Kern[a], Jan-Jan v.d. Vyver[a], Markus Christen[a], Stefano Lecchini[a], Clemens Wagner[b]

[a]*Institut für Neuroinformatik der Universität Zürich UNIZH und der Eidgenössischen Technischen Hochschule Zürich ETHZ, Winterthurerstr. 190, CH-8057 Zürich, Switzerland*

[b]*Physiologisches Institut der Universität Bern, Friedbühlplatz, CH-3000 Bern, Switzerland*

Accepted 12 November 2001

Abstract

Layer IV is believed to be the cortical signal amplifier, for example, of thalamic signals. A previous spiny stellate recurrent network model of this layer is made more realistic by the addition of inhibitory basket neurons. We study the persistence and characteristics of previously observed collective firing behavior, and investigate what additional features would need to be implemented to generate in vivo type neuronal firing. It is shown that neuronal activity is only coarsely synchronized within the network. By applying methods of noise-cleaning, it emerges that the firing of individual neurons is of low-dimensional hyperchaotic nature, as found in the analysis of measured cat in vivo spike trains. In order to reproduce in vivo firing patterns, it is sufficient to have time-varying thalamic input. Conclusions from low-dimensional hyperchaotic behavior of network-embedded neurons are drawn. We interpret observed in vivo pattern-sharpening features of stimuli and outline possible connections to epilepsy. From our results, it follows that emergent global behavior is likely to be the result of the interaction between comparably simple neuronal components, driven by input specificity.

Theme: Motor systems and sensorimotoric integration

Topic: Circuitry and pattern generation

Keywords: Chaos; Coarse synchronization; Noise; Layer IV of neocortex

1. Introduction

In recurrent neuronal circuits, synaptic output is fed back as part of the input stream. Neural connectivity is highly recurrent, but the reasons for this are still poorly understood. In visual cortex, the major excitatory input onto spiny stellate neurons in layer IV arises from neighboring spiny stellate cells and from other cells in the same layer. Only about 6% of the excitatory synapses within layer IV are of (feed-forward) thalamic origin [2,33]. Excitatory neurons are thought to use recurrent excitatory feedback to amplify external network inputs [19,48]. Model studies indicate that recurrent circuits may also shape the receptive field properties of visual cortex neurons [15,44].

The neurons participating in recurrent networks can be divided into classes based on morphology, neurochemistry, and layer location. Interconnections between these classes appear to follow a canonical scheme, that is repeated throughout different cortical areas (the canonical microcircuit [20]). It is believed that computations are carried out predominantly in such local circuits, each of which seems to process a defined area in sensory space [31].

Different types of firing are observed from in vivo intracellular membrane potential measurements of cortical neurons. Following Connors and Gutnick [16], in vivo neuronal firing can be distinguished into regularly spiking, fast spiking, and bursting. Most excitatory neurons are of the regularly spiking type, some of which show an adaptation of the firing rate. Fast spiking cells are generally

*Corresponding author. Tel.: +41-16-353-063; fax: +41-16-353-053.
E-mail address: ruedi@ini.phys.ethz.ch (R. Stoop).

0926-6410/02/$ – see front matter
PII: S0926-6410(01)00123-9

inhibitory neurons. They fire at almost twice the rates of other neurons and virtually do not adapt. When a depolarizing voltage step is applied intracellularly [16,35], the large pyramidal neurons in layer V typically respond with bursting discharge patterns. Under conditions of constant current injection, these neurons display bursting behavior autonomously (intrinsic bursting). The fundamental mechanism leading to bursting is the interplay between at least two dynamics that act on different time scales: A fast process for the generation of single action potentials, and a slower process that provides the switching between repetitive spiking and quiescent phases [12,27,38,50]. Based on specific properties of the fast and of the slow dynamics, Wang and Rinzel [50] introduced a refined classification of bursting.

As a new possibility, we found bursting in simulations of networks of recurrently connected, intrinsically non-bursting neurons [9]. The underlying modelling paradigm is an abstraction of the way spiny stellate neurons are embedded in layer IV of neocortex. These neurons receive feed-forward input from the thalamus and they are densely recurrently connected by excitatory synapses. Analogous to single-cell bursting, processes occurring on different time scales are responsible for network-generated bursting. The fast time scale is given by the fast kinetics of the spike generating sodium and potassium currents, the slower time scale by the feedback excitation from recurrently connected neighbors, which arrives with roughly one interspike interval delay. This is the time it takes for a change in the feed-forward input to modify the firing rate.

An additional, much slower, negative adaptation feedback is responsible for suspending the firing activity. After external input has caused the neurons in the network to start firing, recurrent connections amplify and sustain the firing. A voltage-dependent calcium current rises, which increases the intracellular calcium concentration. This triggers a calcium-dependent potassium current which hyperpolarizes the membrane voltage and terminates the burst.

When, due to intracellular diffusion and buffering, the calcium concentration has decayed, the cell is ready for another cycle. As the collective feedback is produced by the sum of individual synaptic events scattered over time, irregularities emerge in the bursting.

Our previous study [9] considered a recurrent network only of excitatory neurons. For this network, we derived a population model that could reliably describe the occurrence of bursting, but was not able to account for the in-burst irregularities due to the individual properties of the participating neurons. Although widely observed in in vivo measurements, many aspects of the generation and of the functional role of bursting are still unknown. In the present paper, we aim at extending the significance of our findings, by considering a more realistic implementation of layer IV which also includes inhibitory neurons. Although inhibitory synapses account only for 20% of all synapses in the cortex [5], a priori their effect cannot be predicted. We will show that the previously observed bursting phenomenon continues to persists in this setting and we will give an in-depth statistical analysis of the phenomenon. Moreover, we will show that in vivo multiscale bursting (i.e. bursting involving more than two length scales) can reliably be modelled by our recurrent network when choosing appropriate forms of feed-forward input currents (Fig. 1). In our approach, we do not include corticothalamic projections. A detailed discussion of the signal amplification in the thalamus and of possible feed-back phenomena would be beyond the scope of this contribution. We, however, believe that the effects of the corresponding feed-back loop should be within the variety of input patterns that we considered.

2. Materials and methods

2.1. Biophysically plausible network simulation

2.1.1. Excitatory neurons

Our biophysically plausible network simulations are based on simplified compartmental neurons. These model neurons were derived from a reconstructed cat spiny stellate neuron from layer IV of striate cortex, where we used the algorithm of Bush and Sejnowski [13] to simplify the detailed reconstructed geometry of the cell into an eight-compartment version. Compartment geometries were varied randomly ($\pm 10\%$), to account for the variability seen in biological neurons. Each cell was equipped with somatic voltage-dependent conductances, as follows:

- Fast sodium and potassium conductances for the generation of an action potential
- An A-type potassium conductance that linearizes the f–I curve in the perithreshold region
- A high-voltage-activated calcium and a calcium-dependent potassium conductance, for an adaptation of discharge

The conductance models are described in Bernander et al. [7] and Bernander [6]; specific conductance parameters are adopted from Ref. [6].

The numerical simulations were performed using the NEURON simulation environment [30]. The chosen passive properties were $R_m = 5000$ [Ω cm^2] and $C_m = 2$ [μF/cm^2]. Taking into account the inserted active conductances, the input resistance at resting membrane potential was 88 [MΩ]. Synapses were modelled by a current injection into the somatic compartment, where the current function was

$$I_{syn}(t) = \bar{g} \cdot E_{dr} \cdot \frac{t}{\tau_{syn}} e^{1-\frac{t}{\tau_{syn}}}$$

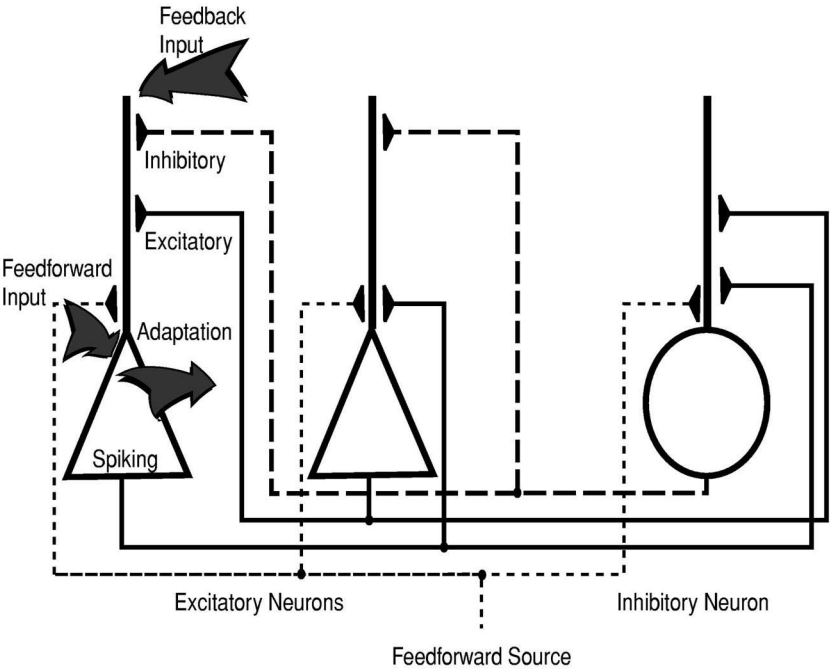

Fig. 1. Architecture of layer IV that was used in our modelling, showing recurrently connected excitatory and inhibitory neurons that receive both feed-forward input and feed-back excitation and inhibition.

where $t_{\mathrm{syn}} = 0.5$ [ms]. The driving potential was fixed to $E_{\mathrm{dr}} = -40$ [mV], to prevent an unrealistic sub-linear summation of synaptic inputs in the simplified cell model. The synaptic peak conductances and latencies varied according to Gaussian distributions, for the conductance with mean $\mu = 7$ and standard deviation $\sigma = 0.84$ [nS], and for the delay with mean $\mu = 1.7$ and $\sigma = 0.7$ [ms]. The variations of the neuron geometries account for the variability of the current–discharge relationships observed in in vivo experiments [3].

2.1.2. Inhibitory neurons

Inhibition was included by adding 20 inhibitory interneurons to the network of 80 excitatory neurons. The morphology of the inhibitory neurons was obtained from a reconstructed basket cell in an analogous way as described for the excitatory neurons. As we wished to investigate the influence of inhibition on the emergence of collective bursting, only inhibitory synapses of the $\mathrm{GABA_A}$ type were included. The synaptic currents triggered by $\mathrm{GABA_B}$ receptors have a long duration, on the order of hundreds of milliseconds, and thus are much longer than the time-scale of the effects of interest here [17]. Inhibitory synapses were placed on the somata of excitatory neurons and had a peak conductance of 1 [nS] [40]. In order to speed up the simulation, synaptic conductances were modelled by a simple exponential function.

To model the currents producing the action potentials, the same ion channels as for the excitatory neurons were used. For matters of simplicity, no calcium and calcium dependent potassium conductances were implemented, because the inhibitory neurons show only very little spike-frequency adaptation.

2.1.3. Connectivity

The connectivity within the network was all-to-all, meaning that each cell is connected to all other cells irrespective of type. All neurons also receive direct monosynaptic input from LGN, which is modelled by a somatic current injection. Depending on the firing patterns to be reproduced, for all neurons, the current injected was either constant or changed as a function of time, synchronously, or individually.

2.2. Quantification of complex behavior

2.2.1. Embedding of time series

In the usual experimental approach to dynamical, possibly chaotic, systems, a scalar time series $x(t)$ of measurements is given. Despite the fact that the underlying dynamical equations governing the system are unknown, by defining m-dimensional vectors $\boldsymbol{x}_i = (x_i,\ x_{i-T} \cdots x_{i-(m-1)T})$ with suitable delays T and embedding dimensions m, a faithful representation of the system is obtained (Whitney's embedding theorem [51] and corresponding generalization to point processes).

2.2.2. Fractal dimensions

Different variants of the fractal dimension concept have been suggested. In Ref. [29], a systematical approach of the different notions of dimension was achieved in terms of generalized dimensions D_q, $q = 1,2,\ldots$. Among them,

the correlation dimension D_2 is of particular interest, since it is possible to implement efficient algorithms for its evaluation. We have used this quantity to characterize the fractal properties of our network response.

2.2.3. Lyapunov exponents

From the time series, we determined the Lyapunov exponents in two ways: by an algorithm that is directly based on average separation of neighboring orbits (yielding only the largest exponent, which will be denoted by λ_{sano}), and from a linear-approximation based algorithm (yielding a set of true and of spurious exponents, from which the spurious need to be identified and discarded [46]). Both approaches are explained in detail in Peinke et al. [37]. Together with bounds from fractal dimension, the first algorithm provides assistance in determining the optimal embedding dimension. In order to exclude spurious exponents, Lyapunov exponents also were calculated from time-inverted time series.

From the non-spurious Lyapunov exponents, the Kaplan–Yorke dimension $D_{\mathrm{K-Y}}$ [37] can be derived. This dimension should qualitatively coincide with the fractal information dimension D_1, and, in general, also with the correlation dimension D_2 [37].

2.2.4. Noise removal

We used our version [32] of the projective noise cleaning technique originally suggested by Grassberger et al. [24].

2.2.5. BDS test

From the correlation integral [25], a non-parametric statistical test for nonlinearity can be derived. The test relies on the expected convergence of the with fractal dimensions associated [37] entropies and tests the null hypothesis that a time series x_t is independent and identically distributed (i.i.d.) against an unspecified alternative. The BDS test, named after Brock and co-workers [10,11], is considered as the most powerful test for distinguishing between stochastic and chaotic processes, where the test works on samples as small as 500 data points.

In our application, we use a simplified BDS test based on the non-normalized statistics:

$$\tilde{W}^{(m)}(N,\epsilon) = C^{(m)}(N,\epsilon) - C^{(1)}(N,\epsilon)^m \quad (1)$$

where $C^{(m)}(N,\epsilon) = \frac{2}{N(N-1)} \sum_{j=1}^{N} \sum_{i=j+1}^{N} \Theta\left(\epsilon - \|x_i - x_j\|\right)$ is the approximation of the correlation dimension in the m-dimensional embedding space by means of the available data, with Θ being the Heaviside step function and $\boldsymbol{x}_i = \boldsymbol{x}(t_i)$, $i = 1, \ldots, N$ the sampled embedded data points. Under the null hypothesis (i.i.d.), $\tilde{W}^{(m)}(N, \epsilon)$ converges towards a normal distribution with zero mean, whereas in the alternative case the empirical mean of $\tilde{W}^{(m)}(N, \epsilon)$ significantly deviates from zero.

2.3. In vivo measurements of cat striate cortex neurons

In vivo data was provided by K.A.C. Martin and J.D. Allison during a series of experiments dedicated to the study of contrast dependence of neural activity in cat visual cortex, in continuation of work published in Ref. [4]. The detailed experimental procedures are outlined in Ref. [34], with the modifications according to Ref. [4]. An adult female cat was fully anesthetized with state being continuously monitored during the experiment. Eyes were pharmacologically stabilized, pupils dilated and contact lenses fitted; eyes were refracted and corrected by lenses to focus on the display. The location of the optical disc of each eye was plotted on a tangent screen with a reversible ophtalmoscope. After termination of recordings, the cat was injected i.v. with an overdose of sodium pentobarbital and perfused through heart with fixatives. For the extracellular recordings, glassy pipettes, a HS-2A headstage preamplifier (Axon Instruments, CA) connected to a Axoprobe 1A amplifier were used. The membrane voltage was filtered at 5 kHz, digitized at 10 kHz (CED 1401) and stored for offline analysis. Before measuring, the receptive field of the cell was hand-plotted on the tangent screen and the optimal stimulus parameters, including orientation, spatial frequency, and temporal frequency, were qualitatively determined using drifting sine wave gratings. Stimulus patterns were generated by a Picasso image synthesizer (InnisFree, Cambridgeshire, UK), controlled by VS software (Cambridge Electronic Design, Cambridge, UK) via a CED 1708 interface. In total, 20 experimental runs were performed and analyzed.

3. Results

The simulation results we report are based upon 80 excitatory spiny stellate and 20 inhibitory basket cells, that were connected using the all-to-all network topology, where, to account for the variability of neuronal responses, morphology and synaptic connections were varied within physiologically know parameter ranges (see Section 2). A detailed check, comparing micro- and macroscopic views (see Ref. [9] for the excitatory part of the network), confirmed that the parameters we used are generic. In the simulations we observed that, despite of the presence of inhibitory neurons, collective bursting behavior, as shown in Fig. 2, emerges. The phenomenon persists over a large part of the physiological data compatible parameter space, where we find that the results derived from the population model in the purely excitatory network, remain qualitatively unchanged (see Ref. [9] for the analysis of the former). Concentrating on the individual neurons' firing, we see that during bursting, the interspike intervals are governed by each neuron's individual current–discharge relationship, on top of which collective bursting behavior is imposed by the strong excitatory couplings. This causes

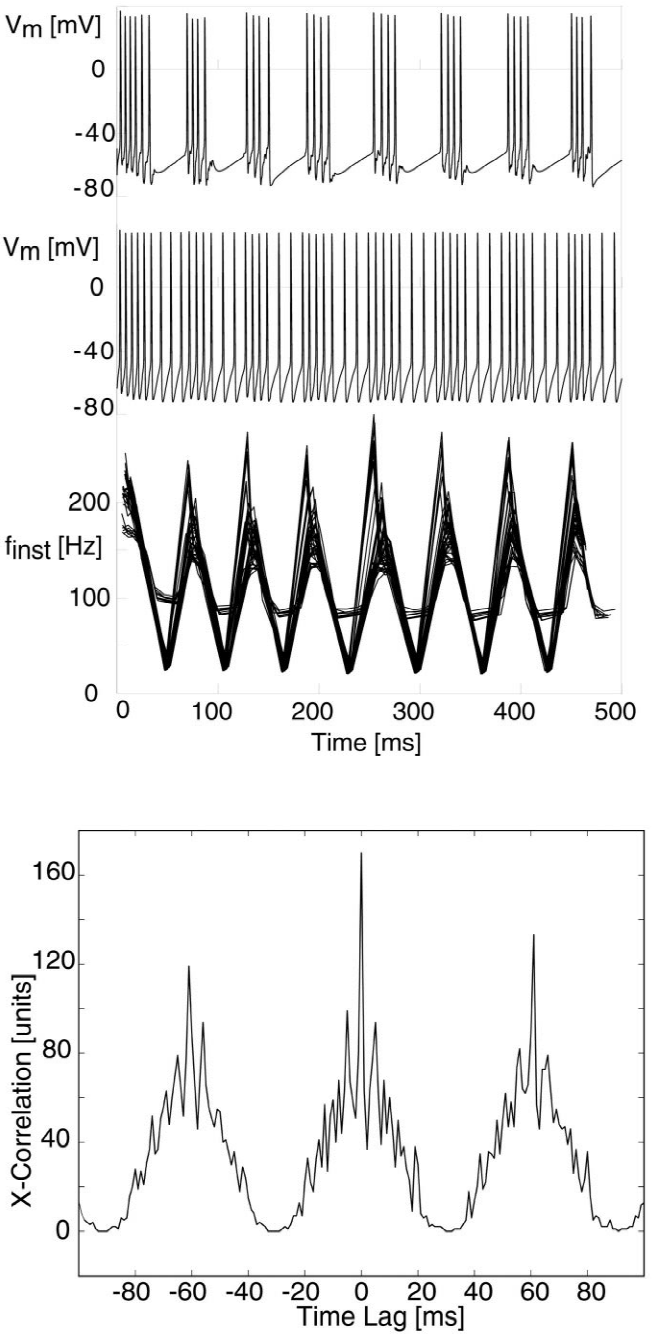

Fig. 2. Collective bursting in an excitatory/inhibitory network of intrinsically non-bursting neurons. Top: spike train of a representative excitatory neuron. Middle: spike train of a representative inhibitory neuron. Bottom: instantaneous firing rates of 32 excitatory/eight inhibitory neurons, showing that they are all roughly synchronized (see text). Lowest: cross-correlogram from two inhibitory neurons showing millisecond synchronization.

the neurons to fire in a coarsely synchronized manner, with variations in the onset of bursting usually within one in-burst spike interval. The question then arises whether these irregularities are of stochastic or of low-dimensional chaotic nature. Only in the latter case can controlling methods [36] be used to transfer information efficiently. The distinction between the two cases is a nontrivial task.

For our analysis, we use the information contained in the embeddings of excitatory/inhibitory interspike intervals. Sequences of intervals obtained from excitatory/inhibitory neurons of the simulated network are shown in Fig. 3Ia and in Fig. 3IIa, respectively. In panels (b) and (c) of these figures, embeddings of interspike intervals of particular neurons expose characteristic aspects of the network activity. From the data, it appears that excitatory neurons have a noisy period-3 behavior, whereas complex, possibly chaotic, behavior seems to emerge in the case of inhibition. Circle-map type plots reveal that, in spite of obvious noisiness, the behavior is quite ordered, with exception of the lowest regions on the diagonal that characterize in-burst spiking. A closer look at these regions reveals an evolution resembling channel motion. Channel motion is well known from models of intermittency [37], where for small initial separation of data points, a strong variation of the time the system is confined to the ‘channel’ state is observed. While differences are small within the channel, outside they are amplified to system size, an observation that is corroborated in our case by the evaluation of the averaged separation of trajectories. The channel motion has a strong similarity to the subthreshold membrane potential evolution. This is the deeper reason why a description of the network activity can be given by a population neuron [9].

In order to more specifically investigate the type of irregularity in the response, we calculated fractal dimensions, Lyapunov exponents and associated entropies from the time series of individual excitatory/inhibitory neurons. In the initial attempt, the fractal dimensions and Lyapunov exponents yielded inconsistent characterizations of the data, and there were strong discrepancies between excitatory and inhibitory neurons. This obstructed a coherent interpretation of the network response. Because the individual neuron characteristics generate deviations from the collective behavior that are similar to noise and because noise affects fractal dimensions far more than the Lyapunov exponents, we applied a novel, powerful noise-cleaning algorithm [24,32] to the data. Subsequently hidden deterministic structures emerged from the noisy attractor (see Fig. 3c). Discarding spurious Lyapunov exponents [37] with the help of fractal dimensions finally yielded a coherent picture of the network dynamics (see Section 2).

The final result is that the simulated system is engaged in a four-dimensional collective dynamical behavior, for inhibitory and for excitatory neurons alike. The behavior in the formerly noise-blurred channel areas is now highly correlated and coherent. The geometric pictures (Fig. 3) agree well with the characterization by Lyapunov exponents and fractal dimensions. When the Lyapunov exponents are evaluated in embedding dimension $d_E = 8$, we

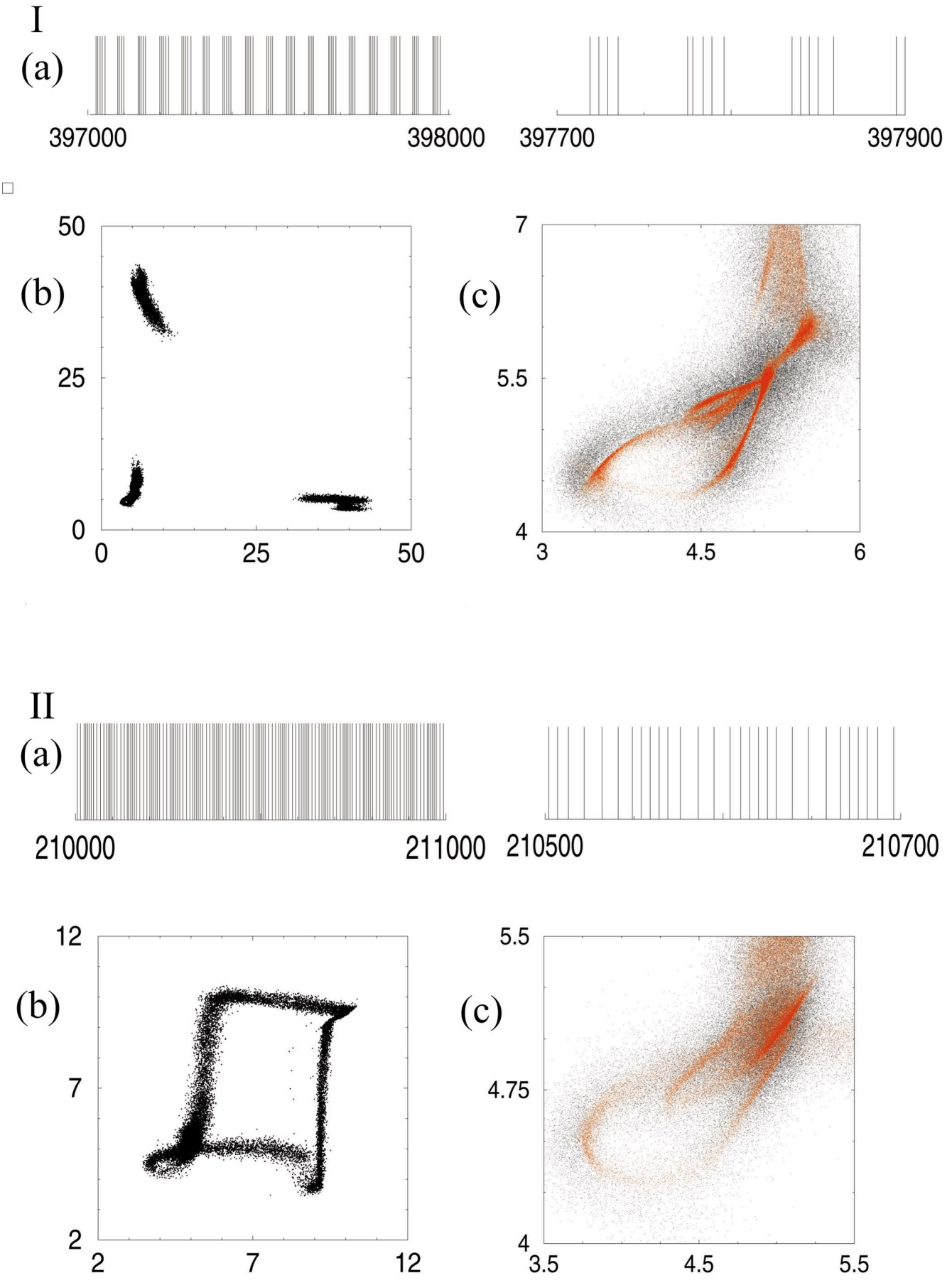
I
(a)
397000
398000
397700
397900
(b)
50
25
0
0
25
50
(c)
7
5.5
4
3
4.5
6
II
(a)
210000
211000
210500
210700
(b)
12
7
2
2
7
12
(c)
5.5
4.75
4
3.5
4.5
5.5

Table 1
Lyapunov exponents and fractal dimensions for the interspike intervals of an inhibitory and an excitatory neuron

	Inhibitory neuron	Excitatory neuron
Noise cleaned $\{\lambda_I\}$, $I = 1\ d_{system}$ ($d_E = 8$, $d_{system} = 4$)	(0.4, 0.12, 0, −1)	(0.5, 0.2, 0, −1)
Noise cleaned D_2	3.5	3.3
Noise cleaned D_{K-Y}	3.4	3.7

obtain typical values $\lambda_{INH} = \{0.4,\ 0.12,\ 0.0,\ -1.0\}$ and $\lambda_{EXC} = \{0.5,\ 0.2,\ 0.0,\ -1.0\}$. The spurious exponents could safely be discarded by matching the Kaplan–Yorke dimensions with the fractal dimensions, which now were constant over a much larger plateau of embedding dimensions. As a result, the Kaplan–Yorke dimensions for the inhibitory neurons $D_{K-Y,\ INH} = 3.5$ and the excitatory neurons $D_{K-Y,\ EXC} = 3.7$, respectively, compared well with the corresponding fractal correlation dimensions $D_{2,\ INH} = 3.5$ and $D_{2,\ EXC} = 3.3$, evaluated over the range of $d_E = \{3,4,5,6,7\}$. The results show that both neuron types, as well as the system as a whole, are in a state of hyperchaos [37,39]. For convenience, the main results are shown in Table 1. Note that the variations of results among individual neurons are smaller than the expected error of the methods [37].

In order to assess the validity of our numerical conclusions, it was important to control how strongly noise-cleaning affects the deterministic nature of the data. We applied a BDS test (see Section 2) to the original and to the noise-cleaned data, and compared the results with a purely stochastic Gaussian having, compared with the original data, identical moments. The results [8] from these tests confirm that the observed irregularities are not of stochastic, but of low-dimensional deterministic nature. Moreover, the differences between the original and noise-cleaned BDS distribution functions are small, with only a minimally sharpened profile for the noise-cleaned data. This implies that noise-cleaning only marginally affected the statistical behavior of the original recordings.

4. Discussion

4.1. Experimental data

Experimental observations show that in vivo bursting is quite a common phenomenon, where often more than two characteristic length scales are observed (= 'multiscale' bursting)[1]. We compared our simulation results with data from extracellular field potential measurements of striate cortex neurons of anesthetized cats, where 20 responses from 10 cells were measured (see Section 2 for details). The stimulation paradigms included spontaneous activity, random dot sequences without coherent motion, or with motion into the cell's preferred direction, where the lengths of the time series varied between 10 000 and 40 000 interspike intervals. For six responses, we found pronounced, nearly horizontal step-like behavior in the dimensional log–log plots [25,37], that are indicative of bursting on different characteristic length-scales, where we distinguished dominantly three (sometimes more) scales. As an illustration, we show in Fig. 4a,b two spike trains from the same neuron corresponding to static random dot and to square-wave grating stimulation, respectively, together with the corresponding log–log plots. In the latter, the structure introduced by the different bursting length scales are clearly visible. A comparison with simulated data suggests that the measured cell is not an intrinsic burster. Rather, it appears that the multiscale structure of the figures is the result of different interacting sub-populations of recurrent networks. In our simulations (see Fig. 4c,d), we were able to reproduce the experimental multiscale bursting by choosing realistically modified forms of the feed-forward current.

The vast majority of multiburst-producing neurons yielded dimensions around the values obtained for our simulation. However, for exceptional data, such as shown in Fig. 4a,b, the spiking behavior was of simpler type

[1]In vivo bursting may arise from three situations that are difficult to distinguish with only single cell measurements. Bursting may originate from intrinsically bursting cells with constant input, it may arise as the direct consequence of a strong oscillatory feed-forward input to the neuron, or it may result from network bursting of the type we consider in our paper. Although these cases could be distinguished by direct somatic current injection [9], for our experimental data, this test could not be performed. We also have no explicit information on whether the measured responses are from excitatory or inhibitory neurons.

Fig. 3. (I) Excitatory spiking activity: (a) Spike trains, (b) 2D-embedding of interspike intervals. (II) Inhibitory spiking: (a) spike trains, (b) 2D-embedding of interspike intervals. Subfigure (c) show magnifications before (black) and after (red) noise cleaning. Noise cleaning uncovers the existence of a perpendicular direction and allows a consistent evaluation of the different probabilistic and dynamical characteristics of the network behavior (see text).

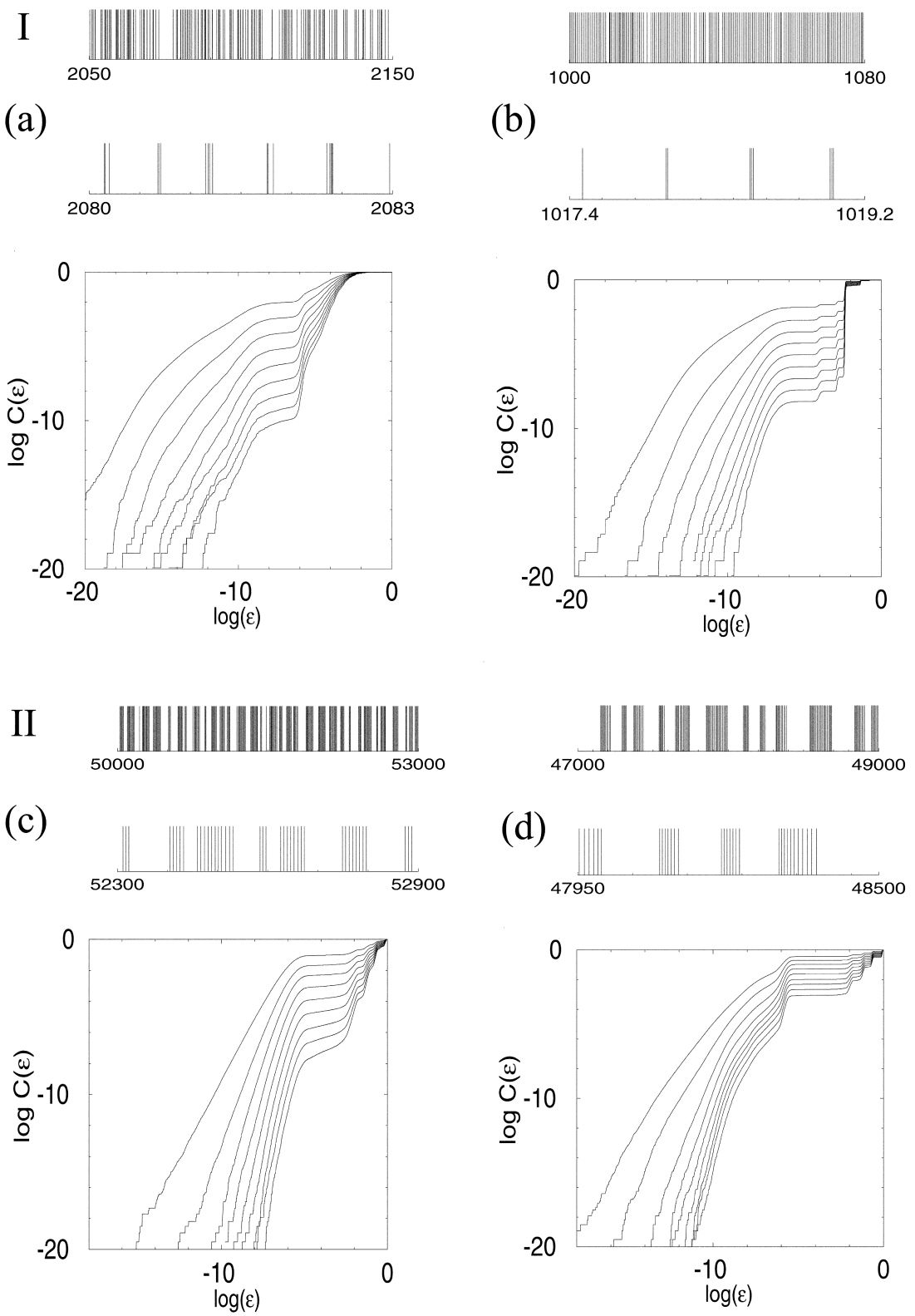

Fig. 4. Experimental and simulated multiscale bursting, represented as spike patterns and by corresponding log–log plots. (I) Experimental in vivo recordings: (a) static random dot stimulation, (b) square-wave grating. According to activity, the measured neuron presumably was inhibitory, but this was not morphologically verified. (II) Simulation results: (c) square-pulses of feed-forward current of same height, individually drawn from five duration lengths (asynchronously pulsed network); (d) square-pulses of feed-forward current of same height, globally drawn from five duration lengths (synchronously pulsed network).

(dimension $d_2 \sim 2.5$, Lyapunov exponents $\lambda_{EXP1} = \{0.8, 0.0, -1.5\}$, $\lambda_{sano1} = \{0.9\}$, and dimension $d_2 \sim 2.4$, $\lambda_{EXP2} = \{0.8, 0.0, -2\}$, $\lambda_{sano2} = \{0.9\}$, respectively). Both experimental files of Fig. 4 originate from the same neuron. This neuron was of particular interest to us because it illustrates neuronal scale-sharpening features due to the stimulus. When we change from random dot (Fig. 4a) to square wave (Fig. 4b) stimulation, the step-like structures become more coherent and settle towards the horizontal. An analysis [47] shows that in the latter state, neurons fire in terms of well-distinguishable, stable firing patterns.

To appreciate the good correspondence between modelling and experiments, it should be noted that the bursting characteristics (emergence of scales) are highly dependent on the specific driving current. In Fig. 5 we show resulting log–log plots for different time-modulated feed-forward driving currents. The comparison suggests that the observed coincidence between simulation and experiment is not artificial but is based on the form of the implemented feed-forward current. In the simplest recurrent network framework of constant thalamic current (Fig. 3), the two dominant length scales correspond to the typical burst length-scale and the interburst length-scale, respectively. Additional length scales may emerge from this simple mechanism (Fig. 5b), as well as from distinct feed-forward currents (that may be generated by strongly connected neuron ensembles that act in parallel but are only weakly coupled (Fig. 5c)). The latter situation, which we associate with the experimental random dot stimulation paradigm, leads to smeared time-scales. In the experimental situation shown in Fig. 4b, stimulation by square-wave grating is used. A natural assumption is that this more specific stimulation paradigm enhances coupling, which would explain how the previously smeared time scales become clearly visible. Additionally, this effect may be enhanced by the chaotic property of the bursting, which will promote synchronization among the different neurons [45]. Finally,

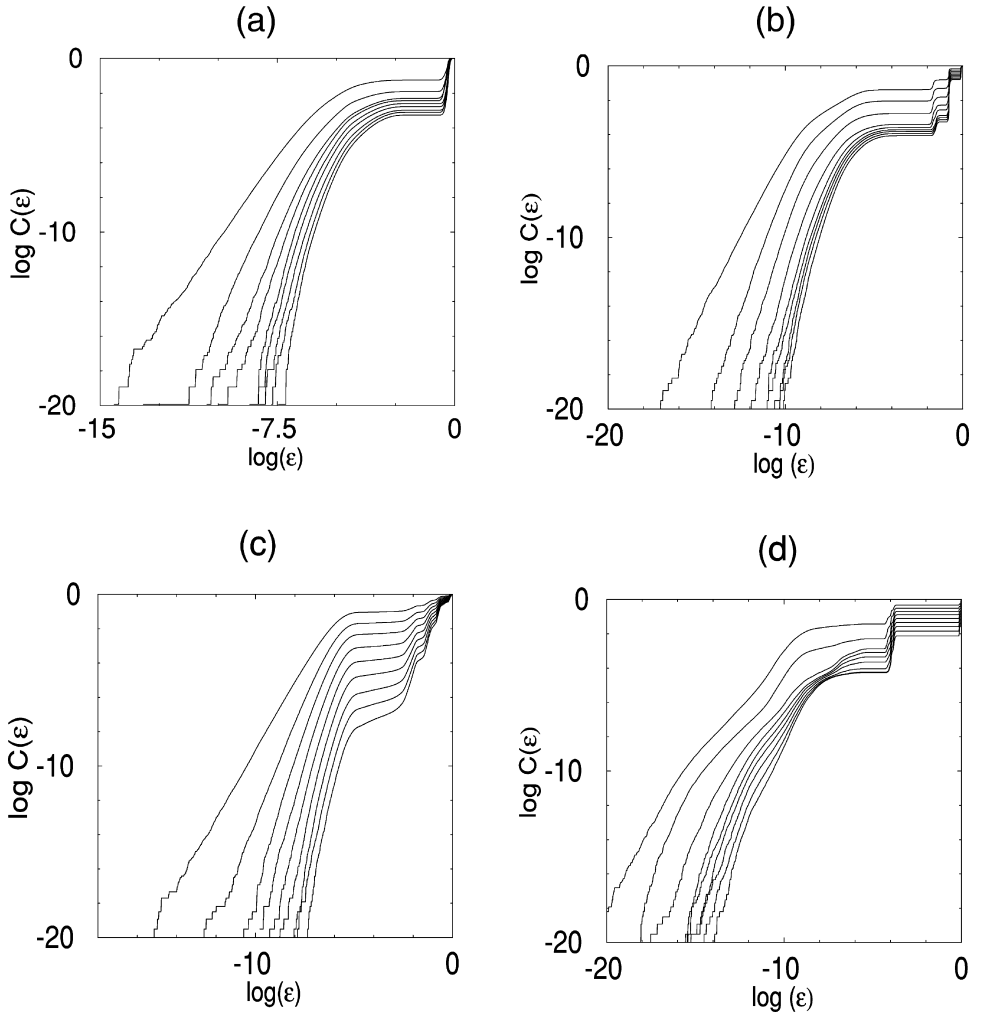

Fig. 5. Characteristic log–log plots for different time-modulated driving currents. (a) Constant current (1 scale, for higher feed forward input, occasionally 2 scales). (b) Square-wave current (3 scales). (c) Five randomly chosen square waves of different length but of equal amplitude. (d) Typical profile obtained from a sinusoidal feed-forward current.

we note that neurons in recurrently coupled networks can be firing normally at biologically plausible, but from bursting conditions different, parameter values [9]. It is also possible that neurons contributing to a smearing of the scales, are finally recruited by the particular stimulus (the square-wave grating). In this way, they may have a considerable influence on the formation of well-distinguishable spiking time-scales.

4.2. Collective synchronization

For our complex system, noise-cleaning was necessary for obtaining a coherent picture. Noise is an inherent property of biological, and in particular of cortical neural network data. Utilizing noise cleaning led to almost identical numerical characterizations of inhibitory and excitatory activities. The latter property can be understood as the effect of strong coupling, which is mediated by the large number of elements in the population pool. This coupling forces distinct excitatory and inhibitory responses into coupling-mediated collective behavior (reflected by the almost identical geometrical shapes of the noise-cleaned attractor structures, see Fig. 3c). Of all the consequences of the morphological and physiological differences from excitatory neurons, only inhibitory firing during excitatory interburst periods withstands this collectivisation. Our results support previously made claims of low dimensional firing behavior [14]. However, the lowest dimensions that were observed in Ref. [14] were not taken at the small distance limit $\epsilon \to 0$, as required in the definition of fractal dimensions, and therefore measure the (macroscopic) stability of firing patterns rather than fractal dimensions (using their approach, we would obtain vanishing dimensions (e.g. in Fig. 4b,d)). Little qualitative changes emerge when we compare the behavior of the mixed excitatory/inhibitory network with that of a purely excitatory network. This indicates that the essence of the conclusions of the population model obtained for the excitatory model also applies in the presence of inhibition [9]. Since the inhibitory and excitatory neurons are synchronized to a high degree, a very efficient network representation in terms of a generalized population model may be obtainable. However, this population model will be unable to account for the chaotic components that we observe in anesthetized cat in vivo data and in corresponding simulations.

4.3. Possible functional roles

In our bursting network, inhibitory neurons are never silent, because they receive monosynaptic excitatory input from LGN and do not adapt to sustained inputs as excitatory neurons do. This is a consequence of the implementation of the corresponding anatomical analysis [4]. Combined with the recurrent network architecture, this results in a firing behavior that is rather similar to that of networks of neurons in already present in simple forms of living systems. One simple example is the central pattern generator (CPG) network of *Tritonia* [21–23]. That different architectural realizations of recurrent networks give rise to similar implementations and generate the same emergent behavior, may have a deeper significance. We propose that this significance be in the fundamental modes of living systems, as expressed by the pattern generator paradigm. The use of temporally precise, strong collective bursting, together with sensitive dependence on initial conditions on short-time scales, may be the result of constraints placed upon living systems. One basic need is to be able to quickly react upon external signals by a significant activity. Multiscale bursting is a highly efficient way of strongly activating exactly tailored, specific, responses (using a multitude of scales to generate specific firing patterns). In parallel, the chaotic property is the expression of the possibility to quickly modify the reaction. In this sense, the almost precise timing of bursts with the option of local modification due to low-dimensional chaotic characteristics, provides a perfect combination of reliability and variability, which are critical requirements for efficient control of important life functions.

To perform, more specifically, computational tasks efficiently, three properties are required: precise timing in the start-up of the process, the possibility of making modifications to patterns at the local level [18], and the ability to achieve this within a sufficiently short time window. To fulfill all of these requirements, synchronized low-dimensional chaotic behavior is ideal, as it can be modified and controlled quickly, and with ease (see, for example, Refs. [28,49]; higher-dimensional chaos cannot be controlled in short time). A more biological interpretation is that each neuron has its own reliable, low-dimensional implementation in the network. When complex information is passed to the brain, it seems to be broken down to allow for a locally low-dimensional, fast processing. This hints at a well-known building principle of complex behavior by means of a large number of simple construction elements (as opposed to complex individual processing units). It is known that by using such architectures, complex behavior emerges [1]. When we want to extrapolate to more global aspects of the behavior of the brain, additional comments are in order. The good agreement between model and experimental data suggests that local networks conforming to our modelling assumptions indeed may be at the backbone of cortical computation. At the same time, our connectivity assumptions imply that the validity of the model will be best met in areas corresponding to the size of one cortical column. The more global behavior of the brain then can be interpreted to be composed of different, mutually weaker coupled local networks. Due to interactions, seemingly more complicated behavior will be displayed, but when measured data is analyzed, the basic construction principle will still emerge.

Bursting behavior and the existence of powerful re-

current excitatory connections, however, also have their danger, as they enhance the possible occurrence of epilepsy [41,52]. Moreover, it was shown that the activity of a single neuron within the population, can change the rhythm of spontaneous discharge [53]. This instability is reminiscent of the low-dimensional chaotic response we have observed. Therefore, it seems possible that epileptic behavior could be triggered by a change of parameters that drive non-bursting neurons into bursting modes (for an overview on the related parameter space for purely excitatory networks, see Ref. [9]), or by a stimulus-induced synchronization, similar to the experimental data shown above. It may well be that under such conditions, inhibitory neurons may no longer prevent, but even enhance the appearance of epilepsy. As a result, the occurrence of epileptic seizures could possibly be explained by strongly synchronized collective bursting contributions by layer IV neurons. However, to establish the exact relation between our observations and epilepsy, much more detailed experimental work on epileptogenetic tissue would need to be conducted. Finally, synchronized activity of assemblies of neurons has been proposed as the solution of the binding problem ([26,43]; for a critical review. see Ref. [42]). From our work, it appears that layer IV synchronization could indeed be involved with the perception of objects. The specific form of encoding in our scheme would, however, differ substantially from the simple synchronization-based encoding proposed by these models of perception.

Acknowledgements

This work was partially supported by the Swiss National Science Foundation and by a KTI contract with Phonak AG. Special thanks go to N. Stoop for computer assistance and for figure preparation.

References

[1] C. Adami, Introduction Into Artificial Life, Springer, Berlin, 1998.
[2] B. Ahmed, J.C. Anderson, R.J. Douglas, K.A.C. Martin, C. Nelson, Polyneuronal innervation of spiny stellate neurons in cat visual cortex, J. Comp. Neurol. 341 (1994) 39–49.
[3] B. Ahmed, J.C. Anderson, R.J. Douglas, K.A.C. Martin, D. Whitteridge, Estimates of the net excitatory currents evoked by visual stimulation of identified neurons in cat visual cortex, Cereb. Cortex 8 (5) (1998) 462–476.
[4] B. Ahmed, J.C. Anderson, K.A.C. Martin, J.C. Nelson, Map of the synapses onto layer 4 basket cells of the primary visual cortex of the cat, J. Comp. Neurol. 380 (1997) 230–242.
[5] C. Beaulieu, M. Colonnier, A laminar analysis of the number of round-asymmetrical and flat-symmetrical synapses on spines, dendritic trunks, and cell bodies in area 17 of the cat, J. Comp. Neurol. 231 (2) (1985) 180–189.
[6] Ö. Bernander, Synaptic integration and its control in neocortical pyramidal cells, PhD thesis, California Institute of Technology, 1993.
[7] Ö. Bernander, R.J. Douglas, K.A.C. Martin, C. Koch, Synaptic background activity influences spatiotemporal integration in single pyramidal cells, Proc. Natl. Acad. Sci. USA 88 (1991) 11569–11573.
[8] D.A. Blank, Firing rate amplification and collective bursting in models of recurrent neocortical networks, PhD thesis, Swiss Federal Institute of Technology ETHZ, 2001.
[9] D.A. Blank, R. Stoop, Collective bursting in populations of intrinsically nonbursting neurons, Z. Naturforsch. A 54 (1999) 617–627.
[10] W. Brock, W. Dechert, J. Scheinkman, A test for independence based on the correlation dimension, University preprints, 1987, See Ref. [11].
[11] W. Brock, D. Hsieh, B. Le Baron, Nonlinear Dynamics, Chaos, And Instability. Statistical Theory and Economic Evidence, Cambridge University Press, Cambridge, 1993.
[12] P.C. Bush, R.J. Douglas, Synchronization of bursting action potential discharge in a model network of neocortical neurons, Neural Comput. 3 (1991) 19–30.
[13] P.C. Bush, T.J. Sejnowski, Reduced compartmental models of neocortical pyramidal cells, J. Neurosci. Methods 46 (2) (1993) 159–166.
[14] A. Celletti, A. Villa, Low-dimensional chaotic attractors in the rat brain, Biol. Cybern. 74 (1996) 387–393.
[15] F.S. Chance, S.B. Nelson, L.F. Abbott, Complex cells as cortically amplified simple cells, Nature Neurosci. 2 (3) (1999) 277–282.
[16] B.W. Connors, M.J. Gutnick, Intrinsic firing patterns of diverse neocortical neurons, Trends Neurosci. 13 (3) (1990) 99–104.
[17] A. Destexhe, T.J. Sejnowski, G protein activation kinetics and spillover of gamma-aminobutyric acid may account for differences between inhibitory responses in the hippocampus and thalamus, Proc. Natl. Acad. Sci. USA 92 (21) (1995) 9515–9519.
[18] M. Dorigo, Learning autonomous robots, IEEE Trans. Syst. Man Cybern. B 26 (3) (1996) 1, Special issue edited by M. Dorigo.
[19] R.J. Douglas, C. Koch, M.A. Mahowald, K.A.C. Martin, H. Suarez, Recurrent excitation in neocortical circuits, Science 269 (1995) 981–985.
[20] R.J. Douglas, K.A.C. Martin, A functional microcircuit for cat visual cortex, J. Physiol. (Lond.) 440 (1991) 735–769.
[21] P.A. Getting, Mechanisms of pattern generation underlying swimming in *Tritonia*. I. Neuronal network formed by monosynaptic connections, J. Neurophysiol. 46 (1) (1981) 65–79.
[22] P.A. Getting, Mechanisms of pattern generation underlying swimming in *Tritonia*. II. Network reconstruction, J. Neurophysiol. 49 (4) (1981) 1017–1035.
[23] P.A. Getting, Mechanisms of pattern generation underlying swimming in *Tritonia*. III. Intrinsic and synaptic mechanisms for delayed excitation, J. Neurophysiol. 49 (4) (1983) 1036–1050.
[24] P. Grassberger, R. Hegger, H. Kantz, C. Schaffrath, T. Schreiber, On noise reduction methods for chaotic data, Chaos 3 (2) (1993) 127–141.
[25] P. Grassberger, I. Procaccia, Dimensions and entropies of strange attractors from a fluctuating dynamics approach, Physica D 13 (1984) 34–54.
[26] C.M. Gray, The temporal correlation hypothesis: Still alive and well, Neuron 24 (1999) 31–47.
[27] J. Guckenheimer, R. Harris-Warrick, J. Peck, A. Willms, Bifurcation, bursting and spike frequency adaptation, J. Comput. Neurosci. 4 (1997) 257–277.
[28] C. Hayes, C. Grebogi, E. Ott, A. Mark, Experimental control of chaos for communication, Phys. Rev. Lett. 73 (1994) 1781–1784.
[29] H.G.E. Hentschel, I. Procaccia, The infinite number of generalized dimensions of fractals and strange attractors, Physica D 8 (1983) 435–444.
[30] M. Hines, A program for simulation of nerve equations with branching geometries, Int. J. Biomed. Comput. 24 (1) (1989) 55–68.

[31] D.H. Hubel, T.N. Wiesel, Receptive fields, binocular interaction and functional architecture in the cat's visual cortex, J. Physiol. (Lond.) 79 (1962) 106–154.
[32] A. Kern, W.-H. Steeb, R. Stoop, Projective noise cleaning with dynamic neighborhood selection, Int. J. Mod. Phys. C 11 (1) (2000) 125–146.
[33] S. LeVay, Synaptic organization of claustral and geniculate afferents to the visual cortex of the cat, J. Neurosci. 6 (12) (1986) 3564–3575.
[34] K.A.C. Martin, D. Whitteridge, Form, function and intracortical projection of spiny neurones in the striate visual cortex of the cat, J. Physiol. (Lond.) 353 (1984) 463–504.
[35] A. Mason, L. Larkman, Correlations between morphology and electrophysiology of pyramidal neurons in slices of rat visual cortex, J. Neurosci. 10 (5) (1990) 1415–1428.
[36] E. Ott, C. Grebogi, J.A. Yorke, Controlling chaos, Phys. Rev. Lett. 64 (1990) 1196–1199.
[37] J. Peinke, J. Parisi, O.E. Roessler, R. Stoop, Encounter With Chaos, Springer, Berlin, 1992.
[38] J. Rinzel, B. Ermentrout, Methods of Neural Modelling: From Synapses to Networks, MIT Press, Cambridge, MA, 1989, Chapter on Analysis of Neural Excitability and Oscillations.
[39] O.E. Roessler, A hyperchaotic attractor, Phys. Lett. A 71 (1979) 155–157.
[40] N. Ropert, R. Miles, H. Korn, Characteristics of miniature inhibitory postsynaptic currents in ca1 pyramidal neurones of rat hippocampus, J. Physiol. (Lond.) 428 (1990) 707–722.
[41] P.A. Schwartzkroin, Cellular electrophysiology of human epilepsy, Epilepsy Res. 17 (3) (1994) 185–201.
[42] M.N. Shadlen, J.A. Movshon, Synchrony unbound: A critical evaluation of the temporal binding hypothesis, Neuron 24 (1999) 67–77.
[43] W. Singer, Time as a coding space?, Curr. Opin. Neurobiol. 9 (1999) 189–194.
[44] D.C. Somers, S.B. Nelson, M. Sur, An emergent model of orientation selectivity in cat visual cortical simple cells, J. Neurosci. 15 (8) (1995) 5448–5465.
[45] R. Stoop, A mathematical approach to mechanisms to synchronize neural activity, Unpublished manuscript.
[46] R. Stoop, P.F. Meier, Evaluation of Lyapunov exponents and scaling functions from time series, J. Opt. Soc. Am. B 5 (1988) 1037–1045.
[47] R. Stoop, J.-J. v.d. Vyver, A. Kern, Detection of noisy and pattern responses in complex systems, in: F. Neerhoff, A. van Staveren, C. Verhoeven (Eds.), Proceedings of the 9th Workshop on Nonlinear Dynamics of Electronic Systems, NDES, Delft University Press, Delft, holland, 2001, pp. 113–116.
[48] H. Suarez, C. Koch, R.J. Douglas, Modelling direction selectivity of simple cells in striate visual cortex within the framework of the canonical microcircuit, J. Neurosci. 15 (10) (1995) 6700–6719.
[49] C. Wagner, R. Stoop, Controlling chaos with simple limiters, Phys. Rev. E (2001) in press;
C. Wagner, R. Stoop, Universal scaling of flat-topped maps, J. Stat. Phys. (2001) in press.
[50] X.J. Wang, J. Rinzel, The Handbook of Brain Theory and Neural Networks, MIT Press, Cambridge, MA, 1995, Chapter on Oscillatory and Bursting Properties of Neurons.
[51] H. Whitney, Ann. Math. 37 (1936) 645.
[52] R.K. Wong, R. Miles, R.D. Traub, Local circuit interactions in synchronization of cortical neurones, J. Exp. Biol. 112 (1984) 169–178.
[53] R.K. Wong, R.D. Traub, R. Miles, Cellular basis of neuronal synchrony in epilepsy, Adv. Neurol. 44 (1986) 583–592.